



RESEARCH LETTER

10.1002/2017GL073071

Key Points:

- The stratospheric polar vortex has weakened and shifted away from the pole in recent decades
- In contrast to recent studies, no evidence is found that sea ice decline has contributed to these trends
- It is proposed that these trends may be primarily a result of internally generated climate variability

Supporting Information:

- Supporting Information S1

Correspondence to:

W. J. M. Seviour,
wseviou1@jhu.edu

Citation:


Seviour, W. J. M. (2017), Weakening and shift of the Arctic stratospheric polar vortex: Internal variability or forced response?, *Geophys. Res. Lett.*, *44*, doi:10.1002/2017GL073071.

Received 14 FEB 2017

Accepted 20 MAR 2017

Accepted article online 27 MAR 2017

Weakening and shift of the Arctic stratospheric polar vortex: Internal variability or forced response?

William J. M. Seviour¹ 

¹Department of Earth and Planetary Sciences, Johns Hopkins University, Baltimore, Maryland, USA

Abstract Recent studies have proposed that the Arctic stratospheric polar vortex has weakened and shifted away from the North Pole during the past three decades. Some of these studies suggest that this trend has been driven by a decline in Arctic sea ice leading to enhanced zonal wave number 1 waves propagating into the stratosphere and that it has in turn contributed to a recent wintertime surface cooling over North America and some parts of Eurasia. Here trends in several measures of the location and strength of the stratospheric polar vortex from 1980 to 2016 are examined in two reanalysis products. All measures show weakening and equatorward shift trends, but only one measure, the vortex centroid latitude, has a trend which is statistically significant at the 95% level in both reanalyses. By comparing large ensembles of historical simulations with preindustrial control simulations for two coupled climate models, the ensemble mean response of the vortex is found to be small relative to internal variability. There is also no relationship between sea ice decline and trends in either vortex location or strength. Despite this, individual ensemble members are found to have vortex trends similar to those observed, indicating that these trends may be primarily a result of natural internally generated climate variability.

Plain Language Summary The Arctic stratospheric polar vortex is a region of strong winds between about 10 and 50 km in altitude encircling the North Pole during winter. Changes in the strength and location of the vortex can affect the weather below. Several recent studies have proposed that the vortex has shifted away from the pole and weakened from 1980 to 2016 as a result of declining sea ice in the Arctic. This study first looks at different measures for vortex changes using two observationally based data sets. Only one measure, the centroid latitude, has a trend which is statistically significant. Next it is investigated whether these trends can be attributed to anthropogenic changes (such as sea ice decline) or natural climate variability by using a large number of climate model simulations. Some of these simulations have increasing greenhouse gases, and others are fixed at preindustrial conditions. Despite large differences in sea ice between the two sets of simulations, there is not a large difference in the likelihood of vortex trends. This suggests that the weakening and shift of the vortex is primarily a result of natural internal climate variability.

1. Introduction

The wintertime extratropical stratosphere is dominated by a region of strong westerly winds, known as the stratospheric polar vortex. Substantial evidence has now been gathered, from both modeling and observational studies, that the strength and location of this vortex can significantly influence surface weather and climate [Gerber *et al.*, 2012; Kidston *et al.*, 2015]. This influence is clearest following the dramatic mid-winter breakup of the vortex in sudden stratospheric warming (SSW) events [Baldwin and Dunkerton, 2001; Mitchell *et al.*, 2013], which have been shown to increase the likelihood of cold-air outbreaks [Kolstad *et al.*, 2010; Tomassini *et al.*, 2012] and tropospheric blocking weather patterns [Woollings *et al.*, 2010]. However, smaller-scale changes in the strength or location of the stratospheric polar vortex can also induce anomalies in the tropospheric circulation below [Ambaum and Hoskins, 2002; Black, 2002], and long-term changes in the vortex may contribute toward trends in tropospheric climate [Scaife *et al.*, 2005; Kim *et al.*, 2014].

Several recent studies have proposed that declining in Arctic sea ice has driven long-term persistent trends in the stratospheric polar vortex. Observational evidence for this link has been suggested from studies of reanalysis data which have found that enhanced upward propagation of wave number 1 and 2 planetary waves, leading to a weakened vortex, occurs at the same time as a decline in sea ice [Jaiser *et al.*, 2013; Kim *et al.*, 2014;

Yang et al., 2016]. Idealized modeling experiments, in which sea ice is perturbed independent of other variables, have also shown a weakened vortex to be associated with low sea ice extent [Kim et al., 2014; Nakamura et al., 2015; Wu and Smith, 2016]. However, in a similar modeling study, Sun et al. [2015] found the effects sea ice loss in the Atlantic and Pacific sectors to cancel, leading to little change in the stratosphere. In addition to these trends in the strength of the vortex, Zhang et al. [2016, hereafter Z16] showed that there has been a trend in the vortex location, consisting of a shift away from the North Pole and toward the Eurasian continent, which they also linked to the decline in Arctic sea ice.

It has been proposed that this shift and weakening of the stratospheric polar vortex has contributed toward trends in surface climate [Kim et al., 2014; Nakamura et al., 2015; Z16], in particular, favoring the cold Eurasian winter surface temperatures [McCusker et al., 2016] which have contrasted with the observed warming over much of the rest of the Northern Hemisphere in recent decades [Hansen et al., 2010]. Since Arctic sea ice decline is thought to be significantly driven by anthropogenic emissions [Bindoff et al., 2013] and projected to continue into the future [Stroeve et al., 2012], it is important to understand whether it is in fact a driver of stratospheric changes. If sea ice decline is a driver, then we may expect the vortex to continue to be displaced and weakened in future, with consequent impacts on surface climate. However, if these stratospheric trends are simply a result of internally generated variability, they may be unlikely to persist into the future.

Here trends are first examined in the strength and location of the Arctic stratospheric polar vortex in two contemporary reanalysis products. Whether anthropogenic emissions and sea ice decline have played a role in driving these observed trends is then investigated by comparing preindustrial control simulations and large ensembles of historical simulations of two coupled climate models. Such large ensembles are necessary in order to determine the role of anthropogenic forcing in the presence of large internal climate variability [Deser et al., 2012]. The following section describes the vortex diagnostics used as well as the reanalysis data and climate models. Section 3 describes the results, and the conclusions are presented in section 4.

2. Data and Methods

2.1. Measures of Polar Vortex Location and Strength

Several different measures of the location of the stratospheric polar vortex have been used by previous studies. In order to test the robustness of observed trends, three such measures are compared here. The first, chosen for direct comparison with Z16, is the fractional area of the Eurasian region (50–70°N, 0–135°E) which is covered by the stratospheric polar vortex. This requires calculating the edge of the polar vortex which, following the method of Nash et al. [1996], is determined as the location of the maximum meridional gradient in potential vorticity (PV), after mapping to “equivalent latitude” coordinates [Butchart and Remsberg, 1986] in which the highest PV isolines are centered around the pole, and PV decreases monotonically toward the equator. Unlike Nash et al. [1996] and Z16, the additional requirement that the vortex edge be close to a peak in the zonal wind is not included; this is needed to remove the effect of thin filaments of PV seen in daily data but not present in the monthly mean data analyzed here. Figure S1 (supporting information) shows the location of the vortex edge calculated from PV averaged from December to February (DJF) on the 475 K isentropic surface from 1979 to 2016. It can be seen that the vortex position and shape is highly variable and that the vortex edge calculated by this method accurately captures the location of the maximum PV gradient. The second method used to determine the stratospheric polar vortex location, also shown by Z16, is simply the latitude of the maximum value of PV in the northern extratropics, again calculated from monthly mean data.

The third measure of the vortex location is the vortex centroid latitude, calculated by the method of two-dimensional moment (or elliptical) diagnostics [Vaugh and Randel, 1999; Mitchell et al., 2011]. In Cartesian (x, y) coordinates, the vortex centroid (\bar{x}, \bar{y}) is defined as

$$(\bar{x}, \bar{y}) = \left(\frac{M_{10}}{M_{00}}, \frac{M_{01}}{M_{00}} \right), \quad (1)$$

where

$$M_{nm} = \iint_S x^n y^m q(x, y) dx dy. \quad (2)$$

Here q is the PV distribution at a particular level and S is the region of the stratospheric polar vortex bounded by the vortex edge which is calculated by the method described above. By transforming back from Cartesian

to spherical coordinates (using a polar stereographic transformation), the centroid latitude can be determined. An advantage of the centroid latitude diagnostic is that it can be adjusted to use geopotential height, rather than PV [Seviour *et al.*, 2013], and so can be easily applied to climate model output [Seviour *et al.*, 2016], which often does not include PV. When the centroid latitude is calculated from geopotential height, the vortex edge is defined as the climatological value of zonal mean geopotential height at 60°N (and the appropriate level). Note that these second and third measures of vortex location do not determine the direction of the vortex shift and so represent less strict constraints than the first measure.

Finally, the strength of the stratospheric polar vortex is determined through the polar cap (60°–90°N) area-weighted average of geopotential height at 50 hPa. A positive trend in the geopotential height represents a weakening of the vortex and a negative trend a strengthening. This metric is very highly correlated with the northern annular mode index [Baldwin and Thompson, 2009] and was used by Kim *et al.* [2014] in their analysis of the effects of changing sea ice on the stratospheric polar vortex.

2.2. Reanalyses and Models

Historical trends are compared in two contemporary reanalysis data sets: the European Centre for Medium-Range Weather Forecasts Interim Reanalysis (ERA-Interim) [Dee *et al.*, 2011] and the Japan Meteorological Agency 55 year Reanalysis (JRA-55) [Harada *et al.*, 2016]. Both reanalyses use four-dimensional variational data assimilation (4-D var) and have been shown to have a relatively consistent representation of extratropical middle-lower stratospheric dynamics [Martineau *et al.*, 2016] and a near-identical climatology of SSW events [Butler *et al.*, 2016]. We limit the analysis to the period 1980–2016, which is common to both reanalysis and therefore allows comparison between them.

In order to attribute the role of anthropogenic forcing in observed trends of the stratospheric polar vortex, preindustrial control simulations are compared with large ensembles of historical simulations for two coupled climate models. The first is the Community Earth System Model version 1 (CESM1) Large Ensemble [Kay *et al.*, 2015], which uses the Community Atmosphere Model version 5 with a horizontal resolution of 0.9° latitude by 1.25° longitude and 30 vertical levels with an uppermost level at 50 km. The model also features fully interactive ocean, sea ice, and land surface components. A 1000 year-long preindustrial control simulation which uses 1850 greenhouse gas concentrations is used to quantify internal variability. The 35-member ensemble of historical simulations is initialized with slightly different initial conditions around 1920, each using identical observed historical greenhouse gas concentrations, aerosols, volcanic eruptions, and other climate forcings until 2005 and following the RCP8.5 scenario [van Vuuren *et al.*, 2011] from 2006 to 2016. For comparison with the reanalysis data, trends are calculated over the 37 year period from 1980 to 2016.

The second set of simulations come from the Canadian Earth System Model version 2 (CanESM2) [Arora *et al.*, 2011], which has an atmospheric component with a spectral horizontal resolution of T63 (~2.81°), 35 vertical levels, and an uppermost level near 48 km. It also features interactive ocean, sea ice, and land surface components. A 995 year-long preindustrial control run with 1850 greenhouse gas concentrations is compared to an ensemble of 50 historical simulations including changes in greenhouse gases, aerosols, land use, and other climate forcings [Sigmond and Fyfe, 2016], using observed values from 1980 to 2005 and also following the RCP8.5 scenario from 2006 to 2016. Similar to the CESM1 ensemble, these are initialized with slightly varying initial conditions at 1950.

3. Results

The three measures of stratospheric polar vortex location are calculated independently on each isentropic level between 430 and 600 K (levels at 430 K, 475 K, 530 K, and 600 K) and averaged to produce the time series shown in Figures 1a–1c for ERA-Interim. Consistent with Z16, there is a positive trend in the fraction of the Eurasian region covered by the stratospheric polar vortex from 1980 to 2016. Trends are shown both for the December–February (DJF) average and for February alone, since Z16 found that statistically significant trends existed only in February. Both DJF and February trends are of the same sign, and approximately similar magnitude, though interannual variability is significantly larger for February. There is also significant interannual correlation of all three location measures, which is strongest for the correlation of the latitude of the PV maximum and the centroid latitude ($r = 0.7$ for DJF). The greatest signal-to-noise ratio is seen for the centroid latitude, for which the ratio of the trend to (detrended) standard deviation is 0.37 decade⁻¹ for DJF (for the latitude of PV maximum this is 0.26 decade⁻¹ and 0.30 decade⁻¹ for the fractional area of Eurasia). Figure 1d also shows the strength of the vortex, as measured by the 50 hPa polar cap geopotential height.

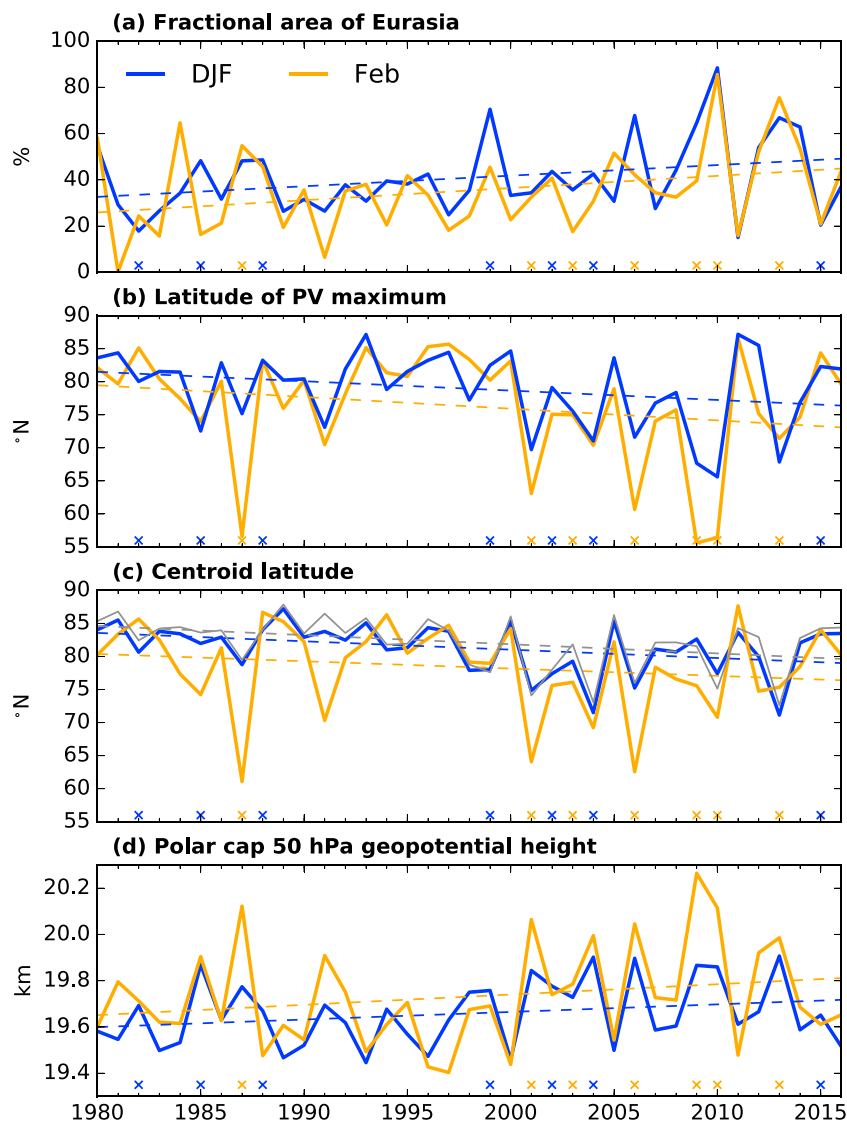


Figure 1. (a–c) Three measures of stratospheric polar vortex location and (d) vortex strength derived from the ERA-Interim reanalysis, calculated from PV on isentropic levels from 430 to 600 K, for February (orange lines) and the December–January (DJF) average (blue lines). Dashed lines show the linear trend from 1980 to 2016, and the gray line in Figure 1c shows the DJF centroid latitude derived from geopotential height. Crosses indicate winters in which an SSW occurred; they are orange if the SSW occurred from 15 January to 15 February and blue if the SSW occurred from 1 December to 15 January.

The positive trends here indicate a weakening of the vortex, and there is an apparent negative correlation between vortex strength and location ($r = -0.82$ with the DJF centroid latitude).

Years in which SSW events occurred between 1 December and 15 February (as given by dates in *Butler et al.* [2016]) are shown in Figure 1. Anomalous high displacement of the vortex toward Eurasia and away from the pole, as well as a weakening of the vortex, can be seen to more often occur in these years in which an SSW occurs. This also highlights the relative dearth of SSW events during the 1990s, a period of a consistently poleward centroid latitude and strong vortex, followed by the high frequency of SSWs in the 2000s. It is apparent, therefore, that these trends in vortex location are to some extent related to the change in SSW frequency.

The trends in stratospheric polar vortex location and strength are shown in Figure 2 for both ERA-Interim and JRA-55 reanalyses. Overall, there is seen to be close agreement between the two reanalyses for trends in all four measures. The only vortex location trends which are found in both reanalyses to be statistically significantly different from zero at the 95% level, according to a Student's *t* test, are the DJF trends in centroid

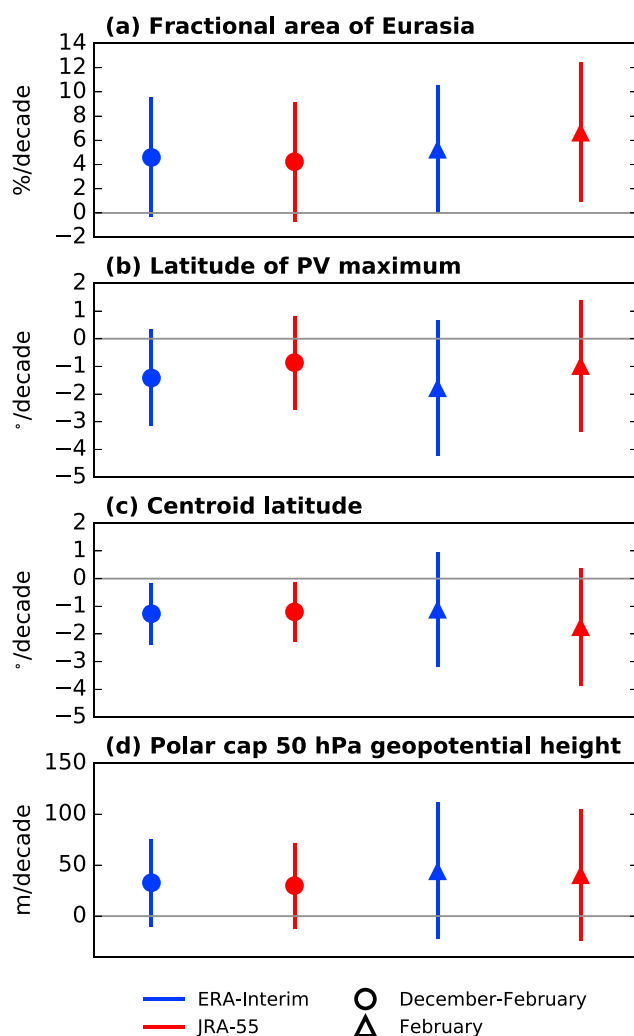


Figure 2. Linear trends from 1980 to 2016 in (a–c) three measures of stratospheric polar vortex location and (d) vortex strength calculated from ERA-Interim and JRA-55 reanalyses using PV on isentropic levels from 430 to 600 K. Trends for both DJF (squares) and February (triangles) are shown. Vertical bars show the 95% uncertainty interval from a Student's t distribution.

latitude for both ERA-Interim ($p = 0.03$) and JRA-55 ($p = 0.02$). The February trend in the fractional area over Eurasia is also statistically significant but only in JRA-55. Years in which SSWs occur are not excluded from this trend analysis, as Z16 did, since these events form part of a continuum of stratospheric polar vortex variability, and several events which are not classified as SSWs also lead to large disturbances in the vortex strength and location [Mitchell *et al.*, 2013; Seviour *et al.*, 2013]. Furthermore, excluding all winters in which any SSW occurred from the DJF averages leaves only 23 years, and none of the trends are then statistically significant. Z16 found the trend in the February fractional area of Eurasia covered by the vortex to be statistically significant at the 95% level in ERA-Interim. Here, however, this trend is not found to be statistically significantly different from zero ($p = 0.07$). If, for more direct comparison with Z16, the same SSW years (1987, 2006, 2009, and 2013) are excluded from the analysis, this trend remains marginally insignificant ($p = 0.051$). This difference with Z16 may result from the slight methodological differences in calculating the vortex edge noted above. Both reanalyses show positive trends in polar cap geopotential height in both DJF and February, indicating a weakening of the vortex, but these trends are not statistically significant.

Since the DJF trend in centroid latitude is the only statistically significant vortex location trend found in both reanalyses, this, along with polar cap geopotential height, will be the focus of the analysis of climate model simulations. The models analyzed here do not output PV so the centroid latitude is calculated from geopotential height at 50 and 70 hPa (similar to the 430–600 K isentropic levels used for PV). Figure 1c shows the DJF

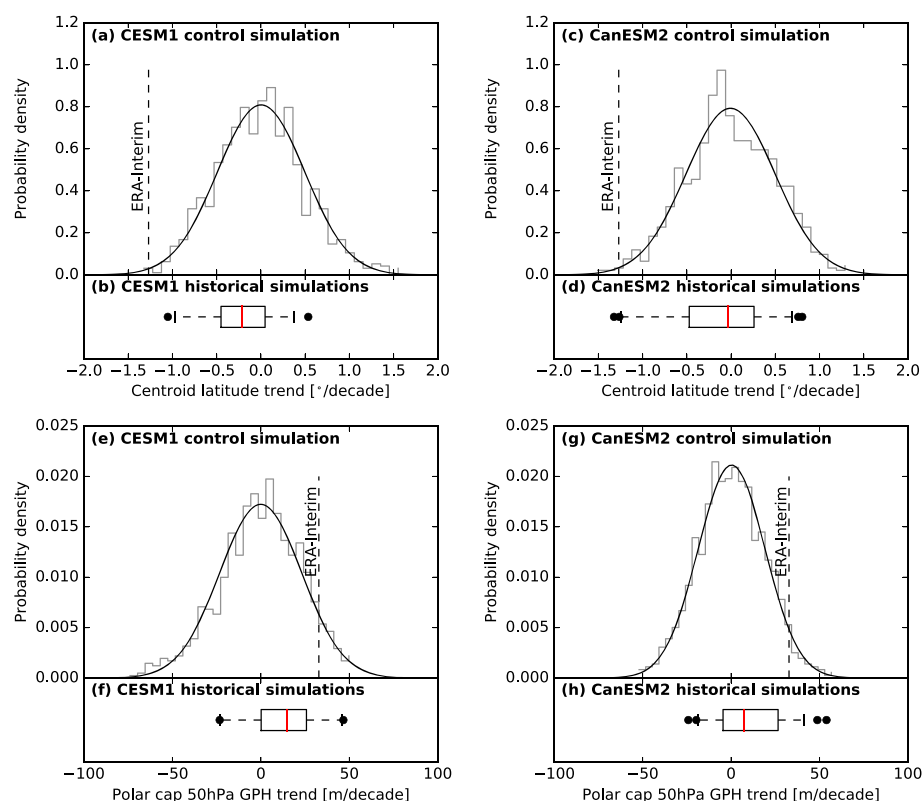


Figure 3. Histograms of 37 year trends in DJF centroid latitude averaged between 50 and 70 hPa (top row) and polar cap 50 hPa geopotential height (bottom row) in the preindustrial control simulation of (a, e) CESM1 and (c, g) CanESM2. A Gaussian fit is also shown. Vertical bars show the magnitude of the 1980–2016 trend in ERA-Interim. Also shown are trends from 1980 to 2016 in (b, f) 35 CESM1 historical simulations and (d, h) 50 CanESM2 historical simulations. Red lines show the mean, the box shows the interquartile range, and the whiskers show the 95% range. Black circles show ensemble members outside this range.

centroid latitude calculated from geopotential height in ERA-Interim (gray line). It can be seen to be highly correlated interannually with the PV-derived centroid latitude ($r = 0.96$), and the 1980–2016 trends in the PV-derived centroid latitude ($1.27^\circ/\text{decade}$) and geopotential height-derived centroid latitude ($1.30^\circ/\text{decade}$) are very similar.

The probability density functions of 37 year trends from the CESM1 and CanESM2 preindustrial control simulations are shown in Figures 3a and 3c (centroid latitude) and 3e and 3g (polar cap geopotential height). These are overlapping trends, calculated by taking values from a 37 year window, moving 1 year at a time. A Gaussian probability distribution provides a good fit in all cases and shows a small probability for a 37 year centroid latitude trend of magnitude at least as large as ERA-Interim (1.0% for CESM1 and 1.2% for CanESM2). For geopotential height these probabilities are larger: 15.6% for CESM1 and 8.6% for CanESM2. It is possible to correct for a bias in model representation of interannual variability by searching for trends with an equal signal-to-noise ratio (i.e., ratio of 37 year trend to (detrended) standard deviation) as in observations (Figure S2, supporting information). The CESM1 centroid latitude has interannual variability which is approximately two thirds of ERA-Interim, and the probability of finding a trend with the same (or larger) signal-to-noise ratio as ERA-Interim is 8.6%. On the other hand, the interannual variability for CanESM2 is slightly larger than ERA-Interim, so the probability of a trend with equal or larger signal-to-noise is just 1.1%. Both CESM1 and CanESM2 have slightly less interannual variability in polar cap geopotential height than ERA-Interim, and the probability of trends with equal or larger signal-to-noise ratio is 21.6% for CESM1 and 13.0% for CanESM2.

Figures 3b, 3d, 3f, and 3h show the distribution of trends in the 35 CESM1 and 50 CanESM2 historical simulations. In the case of CanESM2, the mean of both distributions is near zero, indicating that anthropogenic or other climate forcings have not increased the likelihood of a trend toward a weaker or more displaced stratospheric polar vortex. Indeed, the distributions of CanESM2 control and historical centroid latitude trends are

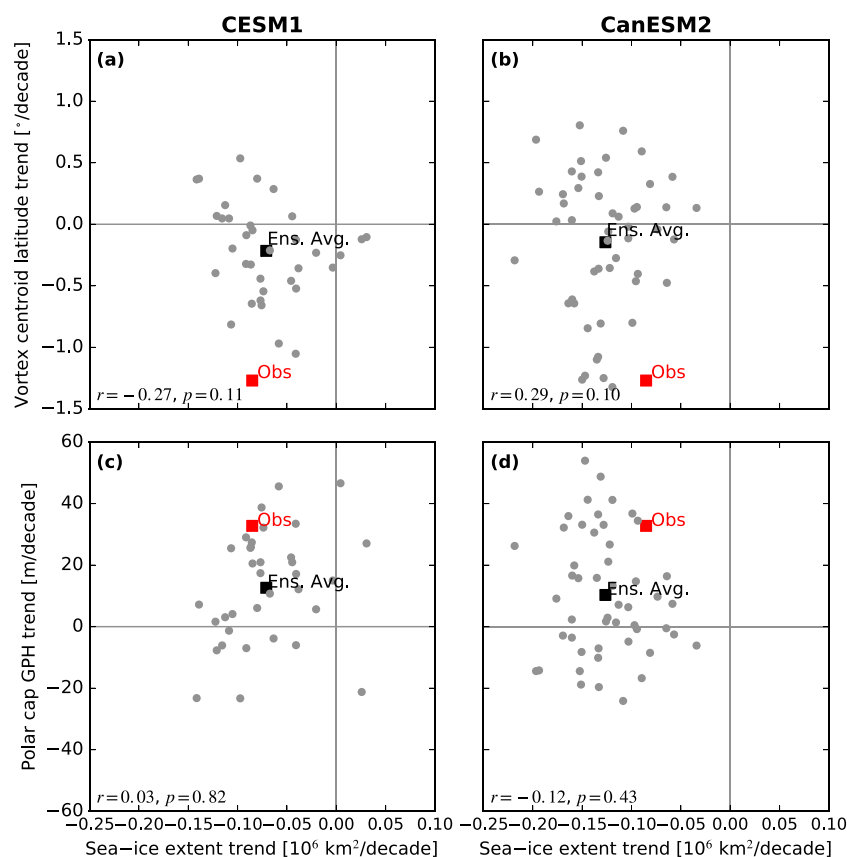


Figure 4. Trends in September–February sea ice extent in the Barents-Kara Sea against (a and b) DJF centroid latitude trends and (c and d) DJF polar cap geopotential height trends from 1980 to 2016 in the CESM1 (Figures 4a and 4c) and CanESM2 (Figures 4b and 4d) historical simulations (gray circles). The black square shows the ensemble average, and the red square shows the observed trend from 1980 to 2016 using HadISST and ERA-Interim data. The correlation coefficient and p value, testing the null hypothesis that the correlation is zero, are shown in the lower left of each panel.

not statistically significantly different according to a Kolmogorov-Smirnov test ($p = 0.42$ for centroid latitude and $p = 0.051$ for geopotential height). In contrast, the CESM1 historical simulations show a greater shift toward a more displaced and weaker vortex, such that the historical ensemble is statistically significantly different from the control ($p = 0.01$ for both centroid latitude and geopotential height). It is important to note, however, that the CESM1 ensemble mean is much less than the observed trend for both metrics, and several individual ensemble members display trends of opposite sign to those observed. As noted in the discussion of reanalysis data, vortex location and strength are highly correlated, and there is also a strong relationship between their trends in individual ensemble members (Figure S3).

It is next examined whether declining sea ice is a cause for a vortex shift or weakening in individual ensemble members, as suggested by previous studies. Figure 4 shows the relationship between 37 year trends in September–February sea ice extent over the Barents-Kara Sea (65–85°N, 30–90°E) and trends in DJF centroid latitude in each of the historical ensemble members. The observed trends are also shown, using sea ice concentrations from the Met Office Hadley Centre Sea Ice and Sea Surface Temperature Data Set (HadISST) [Rayner *et al.*, 2003]. Here sea ice extent is defined as the total area with sea ice concentration greater than 15%. Both models show a clear decline in sea ice extent, with CESM1 having a slightly lower ensemble mean decline than observed and CanESM2 having a slightly greater decline. Both models also capture the observed zonal asymmetry in sea ice changes, with large losses near the Siberian coast but relatively little change near the Canadian and Greenland coasts (Figure S4). Overall, the CESM1 ensemble mean shows sea ice trends which are closer to observations, although the observed trends lie within the ensemble spread of both models. Since CESM1 also shows the largest average stratospheric polar vortex trends, it could be proposed that this is related to its sea ice trends. However, neither model shows any significant correlation between trends

in the polar vortex location or strength and trends in sea ice (this is also true for sea ice trends over the entire Arctic), indicating that these trends are not related.

4. Conclusions and Discussion

In this study trends in the stratospheric polar vortex strength and location have been analyzed in two reanalysis data sets; these show a weakening and equatorward shift of the vortex from 1980 to 2016. However, trends in only one measure of location, the vortex centroid latitude, were found to be statistically significant in both reanalyses. Trends as great as those observed are quite unlikely (about 1% probability for vortex location and 12% for vortex strength) in preindustrial control simulations of two coupled climate models, CESM1 and CanESM2. When considering historical simulations, which include increases in greenhouse gas concentrations, these probabilities increase by a small but significant amount in CESM1 but not in CanESM2. This indicates that anthropogenic emissions may have contributed toward the observed trends, but this contribution is small relative to internal variability. In contrast to recent studies, there is no relationship between trends in vortex strength or location and trends in Arctic sea ice. Therefore, it is proposed that the weakening and shift of the stratospheric polar vortex from 1980 to 2016 may be primarily a result of internal climate variability.

Figures 3 and 4 demonstrate the wide range of trends which can be simulated in climate model ensembles with identical model physics and only varying by their initial conditions. When using small ensemble sizes (such as the 10 year, six-member ensemble of Z16), sampling error may therefore lead to the appearance of a forced response when no such response exists. However, due to the highly nonlinear dynamics of the stratospheric polar vortex, these results do not exclude the possibility of anthropogenically forced changes to the vortex location in future, as suggested by Mitchell *et al.* [2012]. Indeed, analyzing changes in stratospheric polar vortex location and strength in similar ensembles of future climate simulations would be a valuable exercise.

It may be possible that both CESM1 and CanESM2 models fail to simulate realistic coupling between sea ice and the stratospheric circulation, in which case the lack of correlation between the two trends would be expected. However, even if we assume this to be true, the fact that several ensemble members capture stratospheric polar vortex trends similar to those observed would mean that sea ice changes are not a necessary condition to simulate such trends. It should also be noted that both models have uppermost levels near 50 km, which is higher than many “low-top” models, though not as high as many fully stratosphere-resolving (“high-top”) models. Since there is a known lack of dynamical stratospheric variability in low-top models [Charlton-Perez *et al.*, 2013], it is possible that these results are biased relative to the stratosphere-resolving simulations used by Z16. However, CanESM2 actually has a slightly higher frequency of SSW events than observed [Seviour *et al.*, 2016], and the analysis presented here focuses on the middle-lower stratosphere where any biases are smaller. Nonetheless, it will be important to test the robustness of these results in large ensembles of simulations using a fully stratosphere-resolving model.

Acknowledgments

The author thanks John Fyfe, Darryn Waugh, and two anonymous reviewers for their valuable comments.

The CESM Large Ensemble data are publicly available at <http://www.cesm.ucar.edu/projects/community-projects/LENS/> and was performed using computing resources provided by the National Science Foundation, the Computational Information Systems Laboratory, and the National Center for Atmospheric Research. The author acknowledges Environment and Climate Change Canada's Canadian Centre for Climate Modelling and Analysis for executing and making available the CanESM2 large ensemble simulations used in this study and the Canadian Sea Ice and Snow Evolution (CanSISE) Network for proposing the simulations. Code for calculating vortex moment diagnostics is available at <https://github.com/wseviour/vortex-moments>. This work was partially supported by a Frontiers of Earth System Dynamics grant (FESD-1338814) from the U.S. National Science Foundation.

References

- Ambaum, M. H. P., and B. J. Hoskins (2002), The NAO troposphere-stratosphere connection, *J. Clim.*, *15*, 1969–1978.
- Arora, V. K., J. F. Scinocca, G. J. Boer, J. R. Christian, K. L. Denman, G. M. Flato, V. V. Kharin, W. G. Lee, and W. J. Merryfield (2011), Carbon emission limits required to satisfy future representative concentration pathways of greenhouse gases, *Geophys. Res. Lett.*, *38*, L05805, doi:10.1029/2010GL046270.
- Baldwin, M. P., and T. J. Dunkerton (2001), Stratospheric harbingers of anomalous weather regimes, *Science*, *294*, 581–584, doi:10.1126/science.1063315.
- Baldwin, M. P., and D. W. Thompson (2009), A critical comparison of stratosphere-troposphere coupling indices, *Q. J. R. Meteorol. Soc.*, *135*, 1661–1672, doi:10.1002/qj.479.
- Bindoff, N. L., et al. (2013), Detection and attribution of climate change: From global to regional, in *Climate Change 2013: The Physical Science Basis. Contribution of Working Group I to the Fifth Assessment Report of the Intergovernmental Panel on Climate Change*, edited by T. F. Stocker et al., Cambridge Univ. Press, Cambridge, U. K., and New York.
- Black, R. X. (2002), Stratospheric forcing of surface climate in the Arctic Oscillation, *J. Clim.*, *15*, 268–277.
- Butchart, N., and E. E. Remsburg (1986), The area of the stratospheric polar vortex as a diagnostic for tracer transport on an isentropic surface, *J. Atmos. Sci.*, *43*, 1319–1339, doi:10.1175/1520-0469(1986)043<1319:TAOTSP>2.0.CO;2.
- Butler, A. H., J. P. Sjöberg, D. J. Seidel, and K. H. Rosenlof (2016), A sudden stratospheric warming compendium, *Earth Syst. Sci. Data Discuss.*, *9*, 63–76, doi:10.5194/essd-2016-49.
- Charlton-Perez, A. J., et al. (2013), On the lack of stratospheric dynamical variability in low-top versions of the CMIP5 models, *J. Geophys. Res. Atmos.*, *118*, 2494–2505, doi:10.1002/jgrd.50125.
- Dee, D. P., et al. (2011), The ERA-Interim reanalysis: Configuration and performance of the data assimilation system, *Q. J. R. Meteorol. Soc.*, *137*, 553–597, doi:10.1002/qj.828.

- Deser, C., R. Knutti, S. Solomon, and A. S. Phillips (2012), Communication of the role of natural variability in future North American climate, *Nat. Clim. Change*, *2*, 775–779, doi:10.1038/nclimate1562.
- Gerber, E. P., A. Butler, N. Calvo, A. J. Charlton-Perez, M. Giorgetta, E. Manzini, and J. Perlwitz (2012), Assessing and understanding the impact of stratospheric dynamics and variability on the Earth system, *Bull. Am. Meteorol. Soc.*, *93*, 845–859, doi:10.1175/BAMS-D-11-00145.1.
- Hansen, J., R. Ruedy, M. Sato, and K. Lo (2010), Global surface temperature change, *Rev. Geophys.*, *48*, RG4004, doi:10.1029/2010RG000345.
- Harada, Y., H. Kamahori, C. Kobayashi, H. Endo, S. Kobayashi, Y. Ota, H. Onoda, K. Onogi, K. Miyaoka, and K. Takahashi (2016), The JRA-55 reanalysis: Representation of atmospheric circulation and climate variability, *J. Meteorol. Soc. Jpn.*, *94*, 269–302, doi:10.2151/jmsj.2016-015.
- Jaiser, R., K. Dethloff, and D. Handorf (2013), Stratospheric response to Arctic sea ice retreat and associated planetary wave propagation changes, *Tellus A*, *65*, 19375.
- Kay, J. E., et al. (2015), The Community Earth System Model (CESM) large ensemble project: A community resource for studying climate change in the presence of internal climate variability, *Bull. Am. Meteorol. Soc.*, *96*, 1333–1349, doi:10.1175/BAMS-D-13-00255.1.
- Kidston, J., A. A. Scaife, S. C. Hardiman, D. M. Mitchell, N. Butchart, M. P. Baldwin, and L. J. Gray (2015), Stratospheric influence on tropospheric jet streams, storm tracks and surface weather, *Nat. Geosci.*, *8*, 433–440, doi:10.1038/ngeo2424.
- Kim, B.-M., S.-W. Son, S.-K. Min, J.-H. Jeong, S.-J. Kim, X. Zhang, T. Shim, and J.-H. Yoon (2014), Weakening of the stratospheric polar vortex by Arctic sea-ice loss, *Nat. Commun.*, *5*, 4646, doi:10.1038/ncomms5646.
- Kolstad, E. W., T. Breiteig, and A. A. Scaife (2010), The association between stratospheric weak polar vortex events and cold air outbreaks in the Northern Hemisphere, *Q. J. R. Meteorol. Soc.*, *136*, 886–893, doi:10.1002/qj.620.
- Martineau, P., S.-W. Son, and M. Taguchi (2016), Dynamical consistency of reanalysis datasets in the extratropical stratosphere, *J. Clim.*, *29*, 3057–3074, doi:10.1175/JCLI-D-15-0469.1.
- McCusker, K. E., J. C. Fyfe, and M. Sigmond (2016), Twenty-five winters of unexpected Eurasian cooling unlikely due to Arctic sea-ice loss, *Nat. Geosci.*, *9*, 838–842, doi:10.1038/ngeo2820.
- Mitchell, D. M., A. J. Charlton-Perez, and L. J. Gray (2011), Characterizing the variability and extremes of the stratospheric polar vortices using 2D moment analysis, *J. Atmos. Sci.*, *68*, 1194–1213.
- Mitchell, D. M., S. M. Osprey, L. J. Gray, N. Butchart, S. C. Hardiman, A. J. Charlton-Perez, and P. Watson (2012), The effect of climate change on the variability of the Northern Hemisphere stratospheric polar vortex, *J. Atmos. Sci.*, *69*, 2608–2618, doi:10.1175/JAS-D-12-0211.1.
- Mitchell, D. M., L. J. Gray, J. Anstey, M. P. Baldwin, and A. J. Charlton-Perez (2013), The influence of stratospheric vortex displacements and splits on surface climate, *J. Clim.*, *26*, 2668–2682, doi:10.1175/JCLI-D-12-00030.1.
- Nakamura, T., K. Yamazaki, K. Iwamoto, M. Honda, Y. Miyoshi, Y. Ogawa, and J. Ukita (2015), A negative phase shift of the winter AO/NAO due to the recent Arctic sea-ice reduction in late autumn, *J. Geophys. Res. Atmos.*, *120*, 3209–3227, doi:10.1002/2014JD022848.
- Nash, E. R., P. A. Newman, J. E. Rosenfield, and M. R. Schoeberl (1996), An objective determination of the polar vortex using Ertel's potential vorticity, *J. Geophys. Res.*, *101*, 9471–9478, doi:10.1029/96JD000666.
- Rayner, N. A., D. E. Parker, E. B. Horton, C. K. Folland, L. V. Alexander, D. P. Rowell, E. C. Kent, and A. Kaplan (2003), Global analyses of sea surface temperature, sea ice, and night marine air temperature since the late nineteenth century, *J. Geophys. Res.*, *108*(D14), 4407, doi:10.1029/2002JD002670.
- Scaife, A. A., J. R. Knight, G. K. Vallis, and C. K. Folland (2005), A stratospheric influence on the winter NAO and North Atlantic surface climate, *Geophys. Res. Lett.*, *32*, L18715, doi:10.1029/2005GL023226.
- Seviour, W. J. M., D. M. Mitchell, and L. J. Gray (2013), A practical method to identify displaced and split stratospheric polar vortex events, *Geophys. Res. Lett.*, *40*, 5268–5273, doi:10.1002/grl.50927.
- Seviour, W. J. M., L. J. Gray, and D. M. Mitchell (2016), Stratospheric polar vortex splits and displacements in the high-top CMIP5 climate models, *J. Geophys. Res. Atmos.*, *121*, 1400–1413, doi:10.1002/2015JD024178.
- Sigmond, M., and J. C. Fyfe (2016), Tropical Pacific impacts on cooling North American winters, *Nat. Clim. Change*, *6*, 970–974, doi:10.1038/nclimate3069.
- Stroeve, J. C., V. Kattsov, A. Barrett, M. Serreze, T. Pavlova, M. Holland, and W. N. Meier (2012), Trends in Arctic sea ice extent from CMIP5, CMIP3 and observations, *Geophys. Res. Lett.*, *39*, L16502, doi:10.1029/2012GL052676.
- Sun, L., C. Deser, and R. A. Tomas (2015), Mechanisms of stratospheric and tropospheric circulation response to projected Arctic sea ice loss, *J. Clim.*, *28*, 7824–7845, doi:10.1175/JCLI-D-15-0169.1.
- Tomassini, L., E. P. Gerber, M. P. Baldwin, F. Bunzel, and M. Giorgetta (2012), The role of stratosphere-troposphere coupling in the occurrence of extreme winter cold spells over northern Europe, *J. Adv. Model. Earth Syst.*, *4*, M00A03, doi:10.1029/2012MS000177.
- van Vuuren, D. P., et al. (2011), The representative concentration pathways: An overview, *Clim. Change*, *109*, 5–31, doi:10.1007/s10584-011-0148-z.
- Waugh, D. W., and W. J. Randel (1999), Climatology of Arctic and Antarctic polar vortices using elliptical diagnostics, *J. Atmos. Sci.*, *56*, 1594–1613.
- Woollings, T., A. Charlton-Perez, S. Ineson, A. G. Marshall, and G. Masato (2010), Associations between stratospheric variability and tropospheric blocking, *J. Geophys. Res.*, *115*, D06108, doi:10.1029/2009JD012742.
- Wu, Y., and K. L. Smith (2016), Response of northern hemisphere midlatitude circulation to Arctic amplification in a simple atmospheric general circulation model, *J. Clim.*, *29*, 2041–2058, doi:10.1175/JCLI-D-15-0602.1.
- Yang, X.-Y., X. Yuan, and M. Ting (2016), Dynamical link between the Barents-Kara sea ice and the Arctic oscillation, *J. Clim.*, *29*, 5103–5122, doi:10.1175/JCLI-D-15-0669.1.
- Zhang, J., T. Wenshou, M. P. Chipperfield, F. Xie, and J. Huang (2016), Persistent shift of the Arctic polar vortex towards the Eurasian continent in recent decades, *Nat. Clim. Change*, *6*, 1094–1099, doi:10.1038/nclimate3136.